Environmental Fluid Mechanics (2026) 26:9
https://doi.org/10.1007/s10652-026-10073-5

ORIGINAL ARTICLE

# Adjustment time of the lock exchange for a linearly stratified lock and ambient

**Bouke Biemond**[1] · **Robert Jan Labeur**[1]

Received: 28 April 2025 / Accepted: 5 January 2026


**Abstract**
A general theory for the exchange timescale of lock-exchange flows where both the lock and the ambient are stratified has not been established yet. Here, two-dimensional large-eddy simulations of the lock exchange are performed, to quantify the dependence of the adjustment time on linear stratification in the lock and ambient. After validation of the model, simulations show that stratification in the ambient decreases the adjustment time, which is related to an increase of the hydrostatic pressure difference driving the front traveling into the lock. Stratification in the lock also decreases the adjustment time, because a larger stratification is associated with faster internal waves, thereby highlighting the role of internal wave speed in the stratified lock exchange. A reduced model for adjustment time is developed, that extends known relations for front speeds in unstratified conditions to situations with a vertically stratified lock and ambient. Stratification is incorporated by combining its effects on hydrostatic pressure and internal wave speed. This reduced model reproduces the dependence of the adjustment time on the initial density field with reasonable accuracy.

**Keywords** Stratified lock exchange · Adjustment time · Internal waves · Density currents

## 1 Introduction

In the lock exchange experiment, two fluids with different densities are initially separated by a vertical barrier. When the barrier is removed, differences in baroclinic pressure will drive flows in the fluid. This setting has been studied from a large number of perspectives (see [38, 39] and references therein). Most of these studies focus on the characteristics of

✉ Bouke Biemond
w.t.biemond@tudelft.nl

Robert Jan Labeur
r.j.labeur@tudelft.nl

[1] Department of Hydraulic Engineering, Delft University of Technology, Stevinweg 1, 2628 CN Delft, The Netherlands

Published online: 27 January 2026

the bottom front, which forms when the higher density fluid from the lock flows as a density current into the ambient. The bottom front serves as an analog for e.g. sediment plumes, sea breezes and snow avalanches.

In the coastal ocean, differences in salinity and therefore density are abundant due to the freshwater introduced by estuaries. Lock exchange theory is helpful for understanding the dynamics of density fronts, which are e.g. observed around freshwater plumes of estuaries [13, 34, 35]. Another example of conditions that resemble a lock exchange are present when a bay or branch of an estuary attains a different salinity than the connected water body [26], and water between those water bodies is exchanged by density currents. This can have important consequences for pollution dispersal [17] or the extent of salt intrusion in estuaries [12, 28]. A similar situation occurs during the operation of shipping locks, which are locally important for the water exchange between fresh and salt water bodies and therefore for the freshwater resources of coastal regions [7].

The theory of a classical lock exchange, e.g. described by Benjamin [3] and Shin et al. [37], has limitations when serving as an analog for density currents in the coastal ocean. The main difference is the presence of stratification, which is omnipresent in the coastal ocean and has large implications for exchange flows (see e.g. Caulfield [8]). The simplest way to consider stratification is by investigating situations in which there are two layers of fluid in the lock, which have a density jump at their (horizontal) interface [10, 14, 16, 41, 42]. These studies have quantified the effect of stratification on the Froude numbers of the exchange flow and the mixing between the two layers during the exchange. However, natural water bodies often have smooth density gradients in the vertical, due to turbulent vertical mixing, and are therefore better represented by linear stratification than by two distinct layers. For the case that only the ambient is linearly stratified, Maxworthy et al. [27] quantified front speeds of gravity currents and found a dependence on the ratio between the density difference between lock and ambient and the stratification of the ambient. Additionally, this study pointed at the presence of internal waves generated by the gravity current. Dai et al. [11] find that, when the front travels at the bottom, subcritical and supercritical fronts have different characteristics, i.e. the interface between the front and the ambient is characterized by internal waves or Kelvin-Helmholtz billows, respectively. Modeling work by Agrawal et al. [1] shows similar dynamics for a front traveling at the surface. Kokkinos and Prinos [20] describes that this difference between subcritical and supercritical flow impacts the duration of the constant velocity phase of the front. Bolster et al. [5] study intrusions, which travel at the height of neutral buoyancy in the ambient. The maximum front speed is found when this is at the bottom or surface boundary. This is supported by modeling work from Khodkar et al. [19].

These studies show that the physics relevant to the lock exchange with a stratified ambient differs substantially from the situation with a homogeneous ambient. Realistic situations occurring in coastal environments are even more complex as not only the ambient is stratified, but both involved water bodies. For this situation, Maurer et al. [25] find that the speed of an intrusion depends on the ratio of the buoyancy frequencies for the case that there is no difference in depth-averaged density between the lock and the ambient. Ungarish [40] showed, using solutions of the governing one-dimensional shallow-water equations, that stronger stratification in the bottom current is associated with a lower front speed, in situations in which the vertical extent of the bottom front is small compared to the water depth. These conclusions are supported by numerical modeling performed by Goldman et al. [15].

These previous studies either consider exchange flows by an intrusion or by a front traveling along the bottom. A general framework covering both these flow types is however still lacking, which should also include flows having both characteristics—of an intrusion and a front—simultaneously. As a step towards developing such a framework, we perform high-resolution numerical model simulations, in which a semi-closed lock is connected to a (horizontally) unbounded ambient. The lock and ambient are initially linearly stratified, and a range of values for the vertical density gradients and the horizontal density difference between the ambient and lock is considered (see Fig. 1). We quantify the adjustment time, which is defined as the timescale after which equilibrium in the density field of the lock is obtained. The physical analog is, for example, the exchange of a bay or a shipping lock with the coastal ocean. Our research question is: How does the adjustment time of a lock exchange depend on linear stratification initially present in the lock and the ambient?

The remainder of this article is organized as follows. Section 2 presents the description of the numerical model and the set-up of the simulations. Section 3 presents results regarding model validation in terms of front speed, and a sensitivity analysis of the adjustment time using the numerical model. Section 4 presents the derivation of a reduced model that aims to reproduce the dependence of the adjustment time on initial conditions as quantified by the numerical model. The results are discussed in Sect. 5 and conclusions are drawn in Sect. 6.

## 2 Methods

### 2.1 Hydrodynamic model description

The used hydrodynamic model is a finite element based Navier Stokes solver which was first presented and analysed in Labeur and Wells [22]. The model solves the incompressible, non-hydrostatic Navier Stokes equations under the Boussinesq approximation for flow, coupled to a mass conservation equation for density, which read

$$\nabla \cdot \boldsymbol{u} = 0, \tag{1}$$

$$\frac{\partial \boldsymbol{u}}{\partial t} + (\boldsymbol{u} \cdot \nabla)\boldsymbol{u} = -\frac{1}{\rho_0}\nabla p + \nabla \cdot (2\nu \nabla^S \boldsymbol{u}) + \frac{\rho - \rho_0}{\rho_0}\boldsymbol{g}, \tag{2}$$

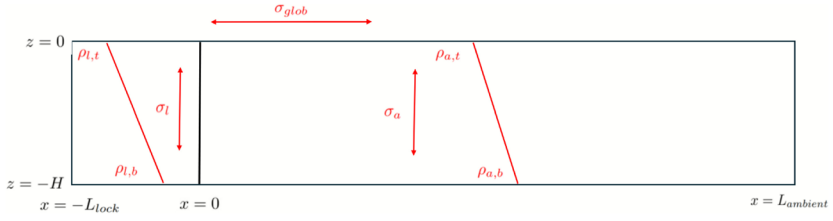


**Fig. 1** Sketch of the model setup. Here, $x$ and $z$ are the horizontal and vertical coordinate, respectively. The undisturbed water depth is denoted by $H$, and the lengths of the lock and ambient are $L_{lock}$ and $L_{ambient}$, respectively. The (initial) density at $z = -H$ (bottom) in the lock is $\rho_{l,b}$, the density at $z = 0$ (top) in the lock is $\rho_{l,t}$; the density at $z = -H$ in the ambient is $\rho_{a,b}$ and the density at $z = 0$ in the ambient is $\rho_{a,t}$. The initial linear (dimensionless) stratifications in the lock and ambient are denoted by $\sigma_l$ and $\sigma_a$, respectively, and the (dimensionless) difference between the depth-averaged initial density in the lock and ambient is $\sigma_{glob}$

$$\frac{\partial \rho}{\partial t} + \boldsymbol{u} \cdot \nabla \rho = \nabla \cdot (\kappa \nabla \rho). \tag{3}$$

Here, u is the velocity vector, $t$ is time, $p$ is pressure, $\nu$ is the viscosity, $\mathrm{g} = (0, 0, -g)^T$ denotes the gravitational acceleration and $\kappa$ is the diffusivity. Furthermore, the symmetric gradient operator is denoted by $\nabla^S$, density is indicated by $\rho$, and the reference density is $\rho_0 = 1000\ \mathrm{kg\ m^{-3}}$. For the domain discretization, unstructured, triangular (2D) or tetrahedral (3D) finite element meshes are used, and the moving free surface is resolved with an Arbitrary Lagrangian–Eulerian (ALE) method. The flow and pressure fields are discretized using discontinuous functions on elements, combined with continuous functions on element interfaces. The latter stabilize the advection terms and the pressure–velocity coupling, while reducing the overall computational complexity to that of a continuous method. Mass and momentum are conserved element wise. For further details and analyses we refer to Labeur and Wells [23, 24].

The model has various options for turbulence closure. Given the grid size used (see next section), a LES method is considered appropriate, for which the WALE model [32] is used. All further numerical model settings are discussed in the next section.

## 2.2 Set-up of the simulations

### 2.2.1 Model validation

To validate the model regarding lock exchange simulations, 2D simulations are set up which mimic experimental setups in Shin et al. [37] and Maxworthy et al. [27]. For Shin et al. [37], this concerns a lock exchange with a non-stratified fluid in the lock and the ambient, for which the density difference between the lock and ambient equals 7 $\mathrm{kg\ m^{-3}}$. We compared the speed of the front in our model with the speed as reported in (Fig. 2 in) Shin et al. [37]. Model validation regarding stratified lock exchanges is performed by comparing the simulations with Maxworthy et al. [27]. Here, front positions as a function of time are given for four experiments in their Fig. 4, where all experiments concern a lock release with a stratified ambient, for different values of stratification of the ambient and density difference between the lock and ambient. We simulated these cases with our model and compared the front speeds.

The other model settings are as follows. For the top boundary, a free surface is used, and for the other walls, a no-slip condition is employed, following Maxworthy et al. [27]. The 2D numerical domain size equals that of the experimental setup, so for comparison with Shin et al. [37] a tank of 2.0 m long and 0.20 m deep is used, while for Maxworthy et al. [27] a tank 2.4 m long and 0.15 m deep is used. The time step is 0.05 s. The grid size is about 1 mm both horizontally and vertically, using an unstructured mesh. The jumps in the initial density profiles are set up using hyperbolic tangent functions. For this, the width of the transition layer $L_{int}$ has to be chosen. We found that this parameter has an effect on the turbulence of the flow which develops later (see Appendix A). Based on the considerations presented in this appendix, we use $L_{int} = 2$ cm.

To track the position of the front, we added a passive tracer to the lock fluid, and the position of the front is defined as the location of the local maximum horizontal gradient of this tracer. Note that with this method the front location is based on the origin of the fluid

(lock or ambient), and both the positions of the surface front and of the bottom front can be tracked.

### 2.2.2 Sensitivity analysis

To control the initial conditions of the linearly stratified lock exchange, we defined three dimensionless parameters. To this end, we first define a maximum density difference $\Delta\rho_{max} = 35$ kg m$^{-3}$, which is (approximately) the density difference between fresh water and seawater. Next, the dimensionless depth-averaged density difference between lock and ambient is

$$\sigma_{glob} = \frac{1}{2\Delta\rho_{max}} \left(\rho_{l,b} + \rho_{l,t} - \rho_{a,b} - \rho_{a,t}\right). \tag{4}$$

Here, $\rho_{l,b}$ and $\rho_{l,t}$ are the densities of the fluid at the bottom and the top in the lock, and $\rho_{a,b}$ and $\rho_{a,t}$ are the bottom and top densities of the ambient, respectively (see also Fig. 1). The linear stratifications in the lock and ambient are quantified as

$$\sigma_l = \frac{\rho_{l,b} - \rho_{l,t}}{\Delta\rho_{max}}, \quad \sigma_a = \frac{\rho_{a,b} - \rho_{a,t}}{\Delta\rho_{max}}, \tag{5}$$

respectively. The maximum value of $\sigma_{glob} = 1$, for which the lock density equals seawater density and the ambient density that of fresh water. The minimum value is $\sigma_{glob} = -1$, where the lock density equals fresh water density and the ambient density that of seawater. The minimum value of $\sigma_l = 0$, for which there is no stratification in the lock, and the maximum value is $\sigma_l = 1$, where the surface density matches the fresh water density and the bottom density is set to the density of seawater. The same range applies to $\sigma_a$. We keep all the densities $\rho_{l,b}, \rho_{l,t}, \rho_{a,b}, \rho_{a,t}$ in the range $\rho_0$ to $\rho_0 + \Delta\rho_{max}$, such that all simulations are representative of situations of a lock exchange which involves (mixtures of) fresh water and seawater. Note that this choice excludes certain combinations of $\sigma_{glob}, \sigma_a$ and $\sigma_l$. For example, the case $\sigma_{glob} = 0.75, \sigma_a = 1$ and $\sigma_l = 1$ is not possible to obtain within these ranges and these situations will therefore not be considered.

Simulations are performed with the model. The water depth is 0.2 m, the length of the lock is 1.0 m and the ambient is 10.0 m long. Numerical settings are identical to those used for the model validation, except that the grid size in the ambient far away from the region of interest is coarser. The simulations are sufficiently long to ensure that the full lock exchange has taken place.

For analysis purposes, we define salinity as $s = \rho - \rho_0$, assuming that all density perturbations are due to salinity. Next, the total amount of salt in the lock is $S_l = \int_V s \, dV$, where $V$ is the volume of the lock. The analysis is performed from the initial time $t = 0$ until time $t = t_{end}$, defined as the point in time when the rate of change in $S_l$ has decreased to 3% of the initial rate.

The dimensionless adjustment time $\tau$ is defined as

$$\tau = \frac{t_{adj}}{t_{scale}}, \quad \text{with} \quad t_{scale} = \frac{2L_{lock} + H}{u}. \tag{6}$$

Here, the (dimensional) adjustment time $t_{adj} = t_{085}/0.85$, where $t_{085}$ is the point of time when 85% of the change in $S_l$ (from the initial value to the value at $t = t_{end}$) has taken place. This threshold of 85% is chosen to avoid being affected by small-scale processes, such as individual Kelvin-Helmholtz billows, which are important for about the last 15% of the adjustment. Some examples and justification for the threshold of 85% are presented in the Supplementary Information Text S1. Furthermore, $t_{scale}$ is the timescale on which the fluid would travel twice the distance $L_{lock}$ with the theoretical maximum speed $u = u_{max} = \frac{1}{2}\sqrt{g'_{max}H}$ [3, 37]. The part $\frac{H}{u}$ in Eq. 6 accounts for the duration of the reflection on the wall at $x = -L_{lock}$. We have defined $g'_{max} = g\frac{\Delta\rho_{max}}{\rho_0}$, and $g = 9.81$ m s$^{-2}$ is the gravitational acceleration.

## 3 Results

### 3.1 Model validation

A comparison of the front position versus time between the experiment described in Shin et al. [37] and our model is given in Fig. 2a. A good agreement is observed: a linear fit to the data yields a front speed of $5.26 \pm 0.03$ and $5.30 \pm 0.04$ cm s$^{-1}$ for the experiment and simulation, respectively, which indicates that the front speeds are indistinguishable for a 95% confidence threshold. Some numerical dispersion is observed in the simulations in regions with strong density gradients. To quantify the consequences, additional simulations were conducted with higher spatial resolution. These yield indistinguishable front speeds, verifying that this behavior has negligible influence on the studied physics. Snapshots of the density field in the model are shown in Fig. 2b–e, which can be compared with the density fields in Fig. 2 in Shin et al. [37]. The most obvious difference is the development of Kelvin-Helmholtz instabilities in our simulation (Fig. 2e), which are less prominent in the experiments. This overestimation of the strength of these features is a well-known property of two-dimensional lock-exchange simulations, but the effects on properties such as the front speeds is thought to be small [9, 27, 33], which is confirmed by our numerical results.

Figure 2f–y show the comparison with experiments presented in Fig. 5 in Maxworthy et al. [27]. For all four experiments, the front speed is well reproduced, which indicates that the model deals well with the front advection in a stratified ambient. There is an offset in the front location for experiment 11 (Fig. 2k–o), which probably originates from the fact that the front position is determined in a different manner here than in Maxworthy et al. [27]. Furthermore, simulated characteristics of the internal wave field are qualitatively in line with those observed in Maxworthy et al. [27], e.g. for supercritical front speeds (Fig. 2f–j) we see no internal waves, but for subcritical front speeds (Fig. 2p–t) an internal wave travels downstream, ahead of the bottom front.

To summarize, the comparison with observations yields satisfactory results and therefore we consider the model suitable to be used for simulations to study the adjustment time of the stratified lock exchange.

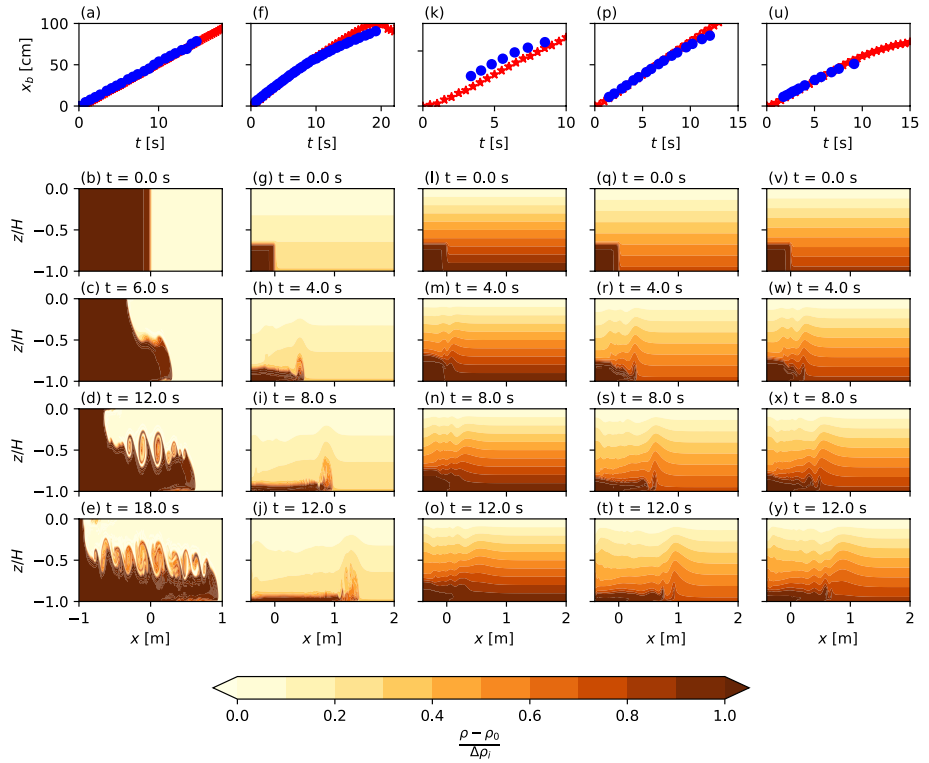


**Fig. 2** **a** Bottom front location $x_b$ versus time, in blue for experimental data from Shin et al. [37] Fig. 2 and in red for the model. **b**–**e** Density fields as a function of $x$ and $z$ for different points in time for the simulation in panel (**a**). Density is normalized by the maximum initial density difference $\Delta\rho_i$. **f**–**j**, **k**–**op**–**t**, **u**–**y**: As **a**–**e**, but for experiments 5, 11, 19 and 22 in Maxworthy et al. [27], respectively

### 3.2 Adjustment time

The adjustment time as a function of $\sigma_{glob}$, the horizontal density difference, is shown in Fig. 3. For $|\sigma_{glob}| = 1$, for which also $\sigma_l = \sigma_a = 0$, the value of $\tau \approx 1.1$ indicates that the adjustment time is about 10–20% larger than the theoretical minimum. Decreasing the absolute value of $\sigma_{glob}$, and considering also the corresponding allowable range of $\sigma_l$ and $\sigma_a$, the adjustment time increases in an approximately symmetric manner around $\sigma_{glob} = 0$. Also, the differences in adjustment time for constant $\sigma_{glob}$ increase for smaller $|\sigma_{glob}|$, indicating that stratification effects become more important for a smaller global horizontal density difference. Note that simulations with $\sigma_{glob} = 0$ are not included in Fig. 3, as the corresponding changes in $S_l$ are always smaller than 3.5%, rendering the determination of $\tau$ inaccurate. Therefore, we exclude this case from our analysis, but will reconsider whether our findings generalize to this situation in Sect. 5.

The effect of $\sigma_a$ and $\sigma_l$ for different values of $\sigma_{glob}$ on adjustment time is shown in Fig. 4. The figure shows that for $|\sigma_{glob}| = 0.50$ or 0.75 the adjustment time is only weakly dependent on $\sigma_a$ and $\sigma_l$. This implies that for relatively large absolute values of $\sigma_{glob}$, the initial stratification of the lock and the ambient is of minor importance and the exchange is

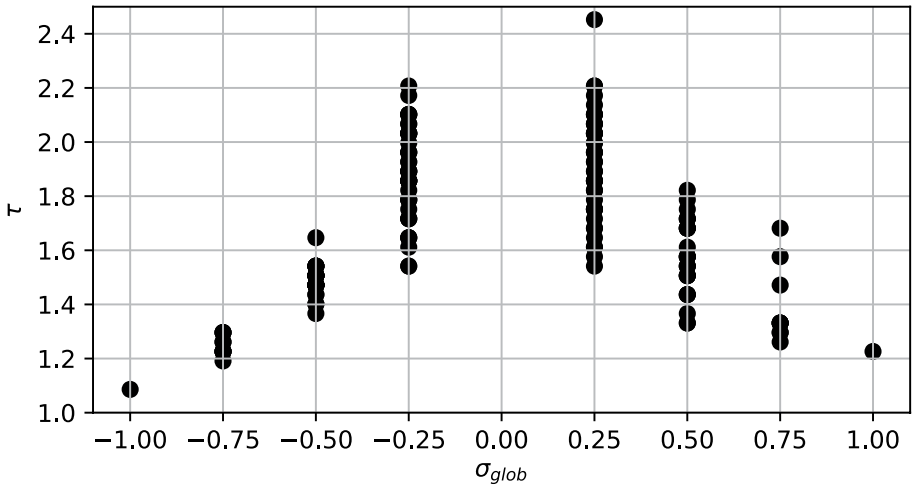


**Fig. 3** Adjustment time $\tau$ as a function of $\sigma_{glob}$ for the simulations with the numerical model, for different values of $\sigma_l$ and $\sigma_a$

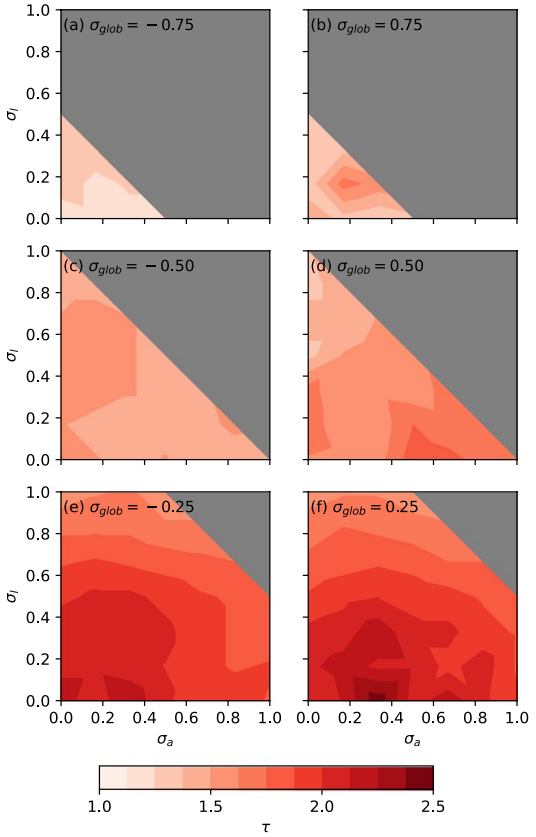


**Fig. 4** **a** Adjustment time $\tau$ as a function of $\sigma_a$ and $\sigma_l$, for $\sigma_{glob} = -0.75$ for the simulations with the numerical model . **b**–**f** As **a**, but for $\sigma_{glob} = 0.75, -0.50, 0.50, -0.25, 0.25$, respectively. The grey areas are parts of the parameter space which cannot be obtained for the associated value of $\sigma_{glob}$ (provided that $\rho_0 < \rho < \rho_0 + \Delta\rho_{max}$)

dominated by the initial horizontal salinity gradient. For $|\sigma_{glob}| = 0.25$, however, the stratification does affect $\tau$ (Fig. 4e and f) substantially. Here, small values of $\sigma_a$ and $\sigma_l$ are associated with large values of $\tau$, while for larger values of either $\sigma_a$ or $\sigma_l$, $\tau$ decreases. In other words, stratification in either the lock or ambient decreases the adjustment time. Extracting patterns in more detail from Fig. 4 is complicated by the uncertainty of determination of adjustment times from the numerical model results, as exemplified in Supplementary Information Text S1.

The dependence of $\tau$ on $\sigma_a$ and $\sigma_l$ is explained by considering the dynamics in more detail. The lock exchange starts with two disturbances traveling in opposite directions. In a stratified environment, the vertical accelerations associated with these disturbances will trigger internal waves. Here, we distinguish between two cases. First, when the speed of the internal wave is smaller than the speed of the associated disturbance, the internal wave is taken over by the disturbance forming a front (or internal bore). This case will be referred to as 'supercritical'. Second, when the internal wave speed is larger than the speed of the initial disturbance, the internal wave will travel away from the disturbance forming a so-called rarefaction wave. We will refer to this case as 'subcritical'. In the following, the dependence of adjustment time on initial conditions will be shown in both supercritical and subcritical conditions.

We focus on the supercritical case first. Fig. 5 visualizes the density fields at different time instances for a simulation with $\sigma_{glob} = 0.25$, $\sigma_a = 0.33$ and $\sigma_l = 0.17$. In panel a, the initial conditions are displayed. After the separation is removed, (panels b and c) a surface and bottom disturbance travel with a constant speed into the lock and the ambient, respectively. Both have the shape of a front (or: internal bore, shock wave) and are properly tracked by the passive tracer. In panel d, the surface front reflects from the horizontal wall at $x = -L_{lock}$. Panels e and f show that after reflection, a disturbance travels in the positive $x$-direction. After about two times the travel time for the front to reach $x = -L_{lock}$ (panel g), the density in the lock reaches a steady state (according to the definition in Sect. 2). This suggests that equilibrium is obtained when the reflected disturbance reaches $x = 0$. Panel h shows that from this moment some changes occur to the density field in the lock, but these barely change the average density of the lock.

Based on these considerations, a good estimate of the adjustment time for supercritical cases is expected to be the time required for a front to travel twice the lock distance (plus a correction for the reflection duration). This adjustment time, referred to as $\tau_{front}$, is computed using Eq. 6 and setting $u = u_{front}$, which is the speed of the front that travels into the lock, either at the free surface (for $\sigma_{glob} > 0$) or at the bottom (for $\sigma_{glob} < 0$). This front speed is derived from the numerical simulation results using a linear fit of the front positions based on the passive tracer.

The results are shown in Fig. 6. Panels a and b show that for $|\sigma_{glob}| \geq 0.75$ the adjustment time is well approximated by $\tau_{front}$ (the maximum difference is smaller than 20%). For $|\sigma_{glob}| = 0.25$ the minimum adjustment time is still correctly represented, however, the maximum values of $\tau_{front}$ exceed the corresponding maximum values of $\tau$. Zooming in on this particular value of $\sigma_{glob}$, Fig. 6c and d show the variation of $\tau_{front}$ with $\sigma_a$ and $\sigma_l$, and panels e and f show the corresponding differences with the numerical model results. In the supercritical regime, that is, the region below the black line, is well approximated by and differences are smaller than 25%. However, in the subcritical regime (the region above the

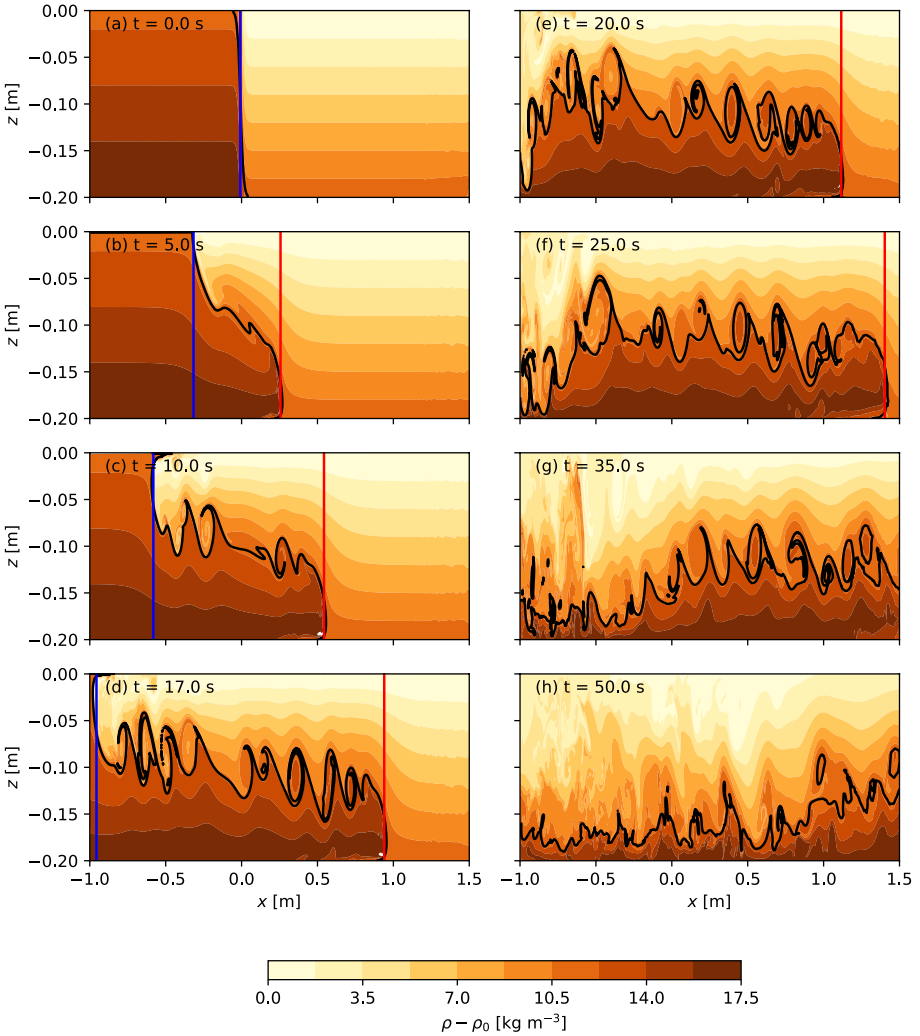


**Fig. 5** Density variation $\rho - \rho_0$ as a function of $x$ and $z$ for different points of time, for a simulation with $\sigma_{glob} = 0.25$, $\sigma_a = 0.33$ and $\sigma_l = 0.17$ (supercritical). The blue and red lines indicate the location of the surface and bottom front, respectively. The black line is the $\rho_0 + \frac{1}{3}\Delta\rho_{max}$ isopycnal

black line), $\tau_{front}$ exceeds $\tau$, indicating that the adjustment is faster in the numerical model than expected based on the front speed.

Considering next the subcritical regime, we visualize density contours for a simulation with a strongly stratified lock ($\sigma_{glob} = 0.25$, $\sigma_a = 0.33$ and $\sigma_l = 1$) in Fig. 7. Panel a shows the initial conditions, in which the strongly stratified lock is visible. Panels b and c show the situation after 4 and 8 s, respectively. The bottom front traveling into the ambient is clearly visible. Inside the lock, the disturbance has the shape of a rarefaction wave. The properties of this rarefaction wave differ from those of the front observed for the supercritical regime. An important difference is that for the supercritical case the front position coincides with the separation between the fluids originating from the ambient and lock, while the rarefaction

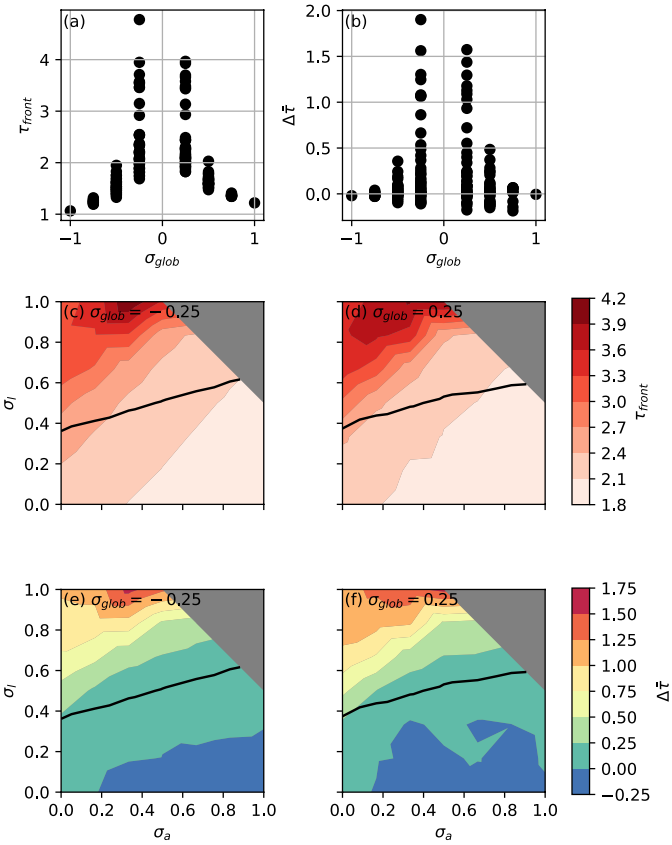


**Fig. 6** **a** Adjustment time based on front speeds $\tau_{front}$, which is an estimation of $\tau$, as a function of $\sigma_{glob}$. **b** As **a**, but for the difference between $\tau$ and $\tau_{front}$, quantified as $\Delta\bar{\tau} = \frac{\tau_{front}-\tau}{\tau}$. **c** Adjustment time $\tau_{front}$ as a function of $\sigma_a$ and $\sigma_l$, for $\sigma_{glob} = -0.25$. The black line indicates the separation between the subcritical and supercritical regime. **d** As **c**, but for $\sigma_{glob} = 0.25$. **e**–**f** As **c**–**d**, but for $\Delta\bar{\tau}$

wave travels ahead of the passive tracer (indicated with blue lines in the figure), transporting only a small amount of ambient fluid into the lock.

Figure 7d shows the rarefaction wave reflecting at the boundary at $x = -L_{lock}$ (while the ambient fluid has reached only $x \approx -0.5L_{lock}$). The reflected wave travels in the positive $x$-direction (panels e and f). At $t = 27.0$ s (panel g), its leading edge arrives at $x = 0$, completing the lock exchange. Indeed, in Fig. 7h, no substantial changes to the density field in the lock have occurred anymore. This suggests that in the subcritical regime the adjustment time can be estimated from Eq. 6 by replacing the velocity scale $u$ with the internal wave speed. Due to the difficulty of extracting the location of the rarefaction wave from the numerical model results, a quantitative assessment of the velocity of the rarefaction wave and associated adjustment time as a function of initial conditions will be given in the next section.

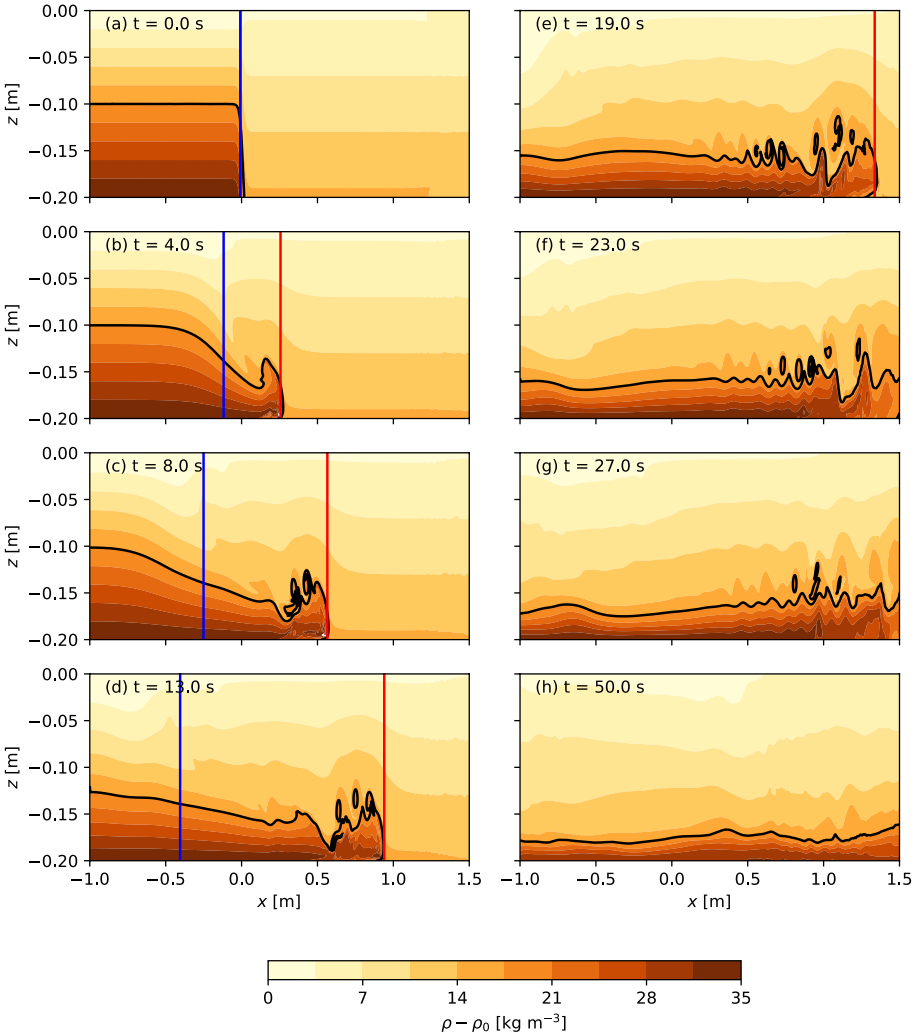


**Fig. 7** As Fig. 5, but for initial conditions $\sigma_{glob} = 0.25$, $\sigma_a = 0.33$ and $\sigma_l = 1$ (subcritical)

## 4 Reduced model for adjustment time

A reduced model for the adjustment time of the lock is proposed. Based on the previous results, this model should discern between cases with either a front or a rarefaction wave as the dominant flow phenomenon for the mass exchange.

### 4.1 Model formulation

To derive an expression for the front speed for the situation where both the ambient and the lock are stratified, an approach from first principles as those in Benjamin [3] and Shin et al. [37] is the most insightful way. Both these methods relate the hydrostatic pressure exerted

on the domain to the change in momentum of the fronts. However, to be able to compute the change in momentum of the front, knowledge about the density distribution in the current is required, which is not obvious from first principles, and additionally is constrained by the fact that the density profile close to the interface between the fluids must remain statically stable. Methods based on a vorticity approach [6, 31] encounter the same restriction for a stratified current. This problem was also noted by Ungarish [40]. The latter study instead uses shallow-water equations for the dynamics of the bottom front, with an imposed density structure. The scope of this theory is limited to gravity currents whose vertical extent is small with respect to the total water depth, such that the return flow is negligible, which is not necessarily true for all cases we consider. Therefore, another assumption will be required to describe the front speed.

To this end, we first consider the supercritical regime for which a front condition for the speed of the bottom front [36] is given by

$$u_b = Fr\sqrt{\frac{\Delta p}{\rho_0}}, \tag{7}$$

where $\Delta p$ is a measure of the pressure difference between the lock and ambient, and $Fr$ is the Froude number of the flow, that is, the ratio of the flow inertia to the applied force. This front condition reduces to the solutions of Benjamin [3], Shin et al. [37] and Borden and Meiburg [6] (if the fluids have constant density) for different values of $Fr$. When using an independently obtained value for $Fr$, this equation provides a value for front speed without the need to solve for momentum or energy conservation. This approach was adopted by a number of studies [4, 18, 39, 40], despite the possible objection that none of the formulations used for the Froude number have a sound theoretical or experimental basis [29]. To avoid using an unsubstantiated formulation of the Froude number, we make the (equally arbitrary, but a posteriori justified) assumption that $Fr$ does not depend on the initial stratification in the lock and ambient, and incorporate the effects of stratification in the hydrostatic pressure difference $\Delta p$. For the situation without stratification, the solution for $u_b$ as presented in Benjamin [3] is used. Subsequently, we solve for $Fr$ in Eq. 7. Back substitution of this result yields for the front speed

$$u_b(\sigma_{glob}, \sigma_a, \sigma_l) = u_{b,0}(\sigma_{glob})\sqrt{\frac{\Delta p(\sigma_{glob}, \sigma_a, \sigma_l)}{\Delta p_0(\sigma_{glob})}}, \tag{8}$$

in which $u_{b,0} = \frac{1}{2}\sqrt{g'_{max}|\sigma_{glob}|H}$ is the front speed in absence of stratification, and $\Delta p_0$ is the pressure difference in absence of stratification (that is, as in Benjamin [3]).

The next step is to evaluate the pressure difference in Eq. 8. The relevant parameter is the initial horizontal force per unit depth, which is obtained by integrating the initial hydrostatic pressure difference over depth, divided by the depth. This force drives the acceleration of the fluid, which directly governs the front speed. For unstratified conditions this yields

$$\Delta p_0 = -\frac{1}{2}gH\Delta\rho_{max}\sigma_{glob}, \tag{9}$$

and for linearly stratified conditions we obtain

$$\Delta p = gH\Delta\rho_{max}\left(\frac{1}{12}(\sigma_1 - \sigma_2) - \frac{1}{2}\sigma_{glob}\right). \tag{10}$$

Here and in the following, we have used subscripts 1 and 2 to indicate the regions (lock or ambient) with the lowest and highest depth-averaged density, respectively.

Next, the speed of the surface front needs to be computed. In unstratified conditions this is equal to the speed of the bottom front [3], but this is not necessarily the case for stratified conditions (Fig. 7). However, the symmetry between the adjustment times for $\sigma_{glob} < 0$ (bottom front travels into lock) and $\sigma_{glob} > 0$ (surface front travels into lock) suggests that we can use the same formulation for the surface front as for the bottom front. Therefore, Eq. 8, where $\sigma_{glob}$ is replaced with $-\sigma_{glob}$, is used for the surface front speed as well, which closes the model formulation for the supercritical regime.

To complete the model for the adjustment time the subcritical regime needs to be incorporated, which is characterized by the occurrence of rarefaction waves. A good estimation of the speed of a rarefaction wave is that of the fastest internal wave. In linearly stratified conditions, this is well approximated by $u_{iw} = \frac{NH}{\pi}$ [2], in which $N = \sqrt{-\frac{g}{\rho_0}\frac{\partial\rho}{\partial z}}$ is the buoyancy frequency. The relevant vertical density gradient is the initial density gradient in the lock, as this is the medium in which the rarefaction waves travel. Inserting this in the expression for the internal wave speed yields

$$u_{iw} = \frac{\sqrt{g'_{max}\sigma_l H}}{\pi}. \tag{11}$$

The model for adjustment times is now complete. In summary, for a lock exchange with positive $\sigma_{glob}$ (lock has a higher density than ambient), a front and an internal wave travel into the lock. The maximum of the associated speeds (as given by Eqs. 8 and 11) is inserted in Eq. 6 and this gives the adjustment time from the reduced model $t_{red}$, which reads

$$t_{red} = \frac{2L_{lock} + H}{\max(u_b, u_{iw})}, \quad \tau_{red} = \frac{t_{red}}{t_{scale}}. \tag{12}$$

The same procedure applies for negative $\sigma_{glob}$ (ambient has a higher density than lock), but now the speed of the bottom front is used instead of the surface front in Eq. 8.

### 4.2 Comparison with numerical model results

Figure 8a provides an overview of the adjustment times $\tau_{red}$ computed with the reduced model. Panel b shows a quantitative comparison between the adjustment time observed in the numerical model and the estimate from the reduced model. The relative difference is smaller than 10% for 66% of the parameter space. However, differences up to about 30% occur, in particular for lower values of $|\sigma_{glob}|$. To examine these situations more closely, panels c and d show the dependence of $\tau_{res}$ on $\sigma_a$ and $\sigma_l$ for $|\sigma_{glob}| = 0.25$. Generally, this dependence is consistent with the corresponding numerical model results shown in Fig. 4e

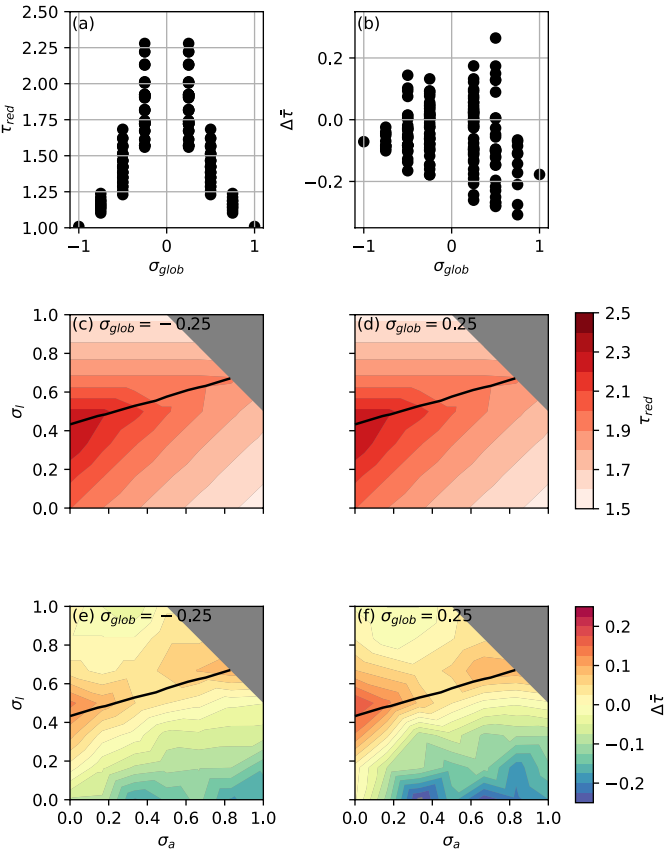


**Fig. 8** **a** The adjustment time $\tau_{red}$ as computed with the reduced model, as a function of $\sigma_{glob}$. **b** The relative difference in adjustment time $\Delta\bar{\tau} = \frac{\tau_{red}-\tau}{\tau}$ as a function of $\sigma_{glob}$. **c** Adjustment time $\tau_{red}$ as a function of $\sigma_a$ and $\sigma_l$, for $\sigma_{glob} = -0.25$. The black line indicates the separation between the subcritical and supercritical regime. **d** As **c**, but for $\sigma_{glob} = 0.25$. **e** The relative difference in adjustment time $\Delta\bar{\tau}$ as a function of $\sigma_a$ and $\sigma_l$ for $\sigma_{glob} = -0.25$. **f** As **e**, but for $\sigma_{glob} = 0.25$

and f, that is, maximum adjustment time for an unstratified ambient, and decreasing values for increasing lock stratification in the subcritical regime and increasing ambient stratification in the supercritical regime. The relatively large deviations occur for small values of $\sigma_l$, viz, weakly stratified locks (Fig. 8e and f).

Given the simplicity of the reduced model, its agreement with the numerical model is reasonably good. The differences mentioned are possibly explained by considering the effect of lock stratification on turbulence. As stratification suppresses turbulence, stronger lock stratification is associated with weaker turbulence production during the exchange, as compared to situations with weakly stratified locks. This is illustrated in Supplementary Information Figs. S3 and S4. While turbulence has little impact on the front speed [9, 27, 33], it seems to affect horizontal mass transport after the reflected internal bore reaches the lock entrance ($x = 0$). Our simulations show that at this point of time the magnitude of the horizontal flow at this location decreases abruptly, but a residual vertical circulation still persists for some time. In cases where vertical mixing has been weak during the exchange, most of the

lock fluid has been replaced by fluid having the ambient density. Consequently, the net mass transport due to the residual flow is negligible and the exchange ceases abruptly. In these situations (i.e., with strong lock stratification), the adjustment time in the numerical model is predicted well by the reduced model. In contrast, when vertical mixing has been strong during the exchange, fluid is observed in the lock with intermediate density. In these situations the residual circulation would involve a net exchange of mass - as the fluid transported out of the lock has a different density than the fluid transported into the lock. This suggests that for relatively weak lock stratification the exchange of mass continues some time after the bore has left the lock, implying an under prediction of the adjustment time by the reduced model (which does not include this effect). The details of the this mechanism are considered a topic for future study, as well as other mechanisms that potentially affect the adjustment time of weakly stratified locks.

### 4.3 Comparison with literature

In the following our results for front speed (and thus adjustment time) are compared to literature values. The classical relation between horizontal density difference and front speed $u \sim \sqrt{\frac{\rho_2-\rho_1}{\rho_0}}$ [3, 37], developed for an unstratified lock and ambient, holds when the stratification is weak with respect to the horizontal density difference. A generalization of the front speed for a stratified ambient is presented in Linden [21], who finds

$$u = u_{b,0}\sqrt{1 - \frac{3}{4}\frac{\rho_{1,b} - \rho_{1,t}}{\rho_2 - \rho_{1,t}}}. \tag{13}$$

The front speed given in this equation is plotted as a function of stratification in the lock and ambient in Fig. 9b. The relation between front speed and stratification in the ambient is similar to that observed in our numerical (Fig. 9a) and reduced models. By construction, Eq. 13 does not include the effects of stratification in the lock. For a homogeneous intrusion into a stratified ambient, Bolster et al. [5] derives an expression based on energy consider-

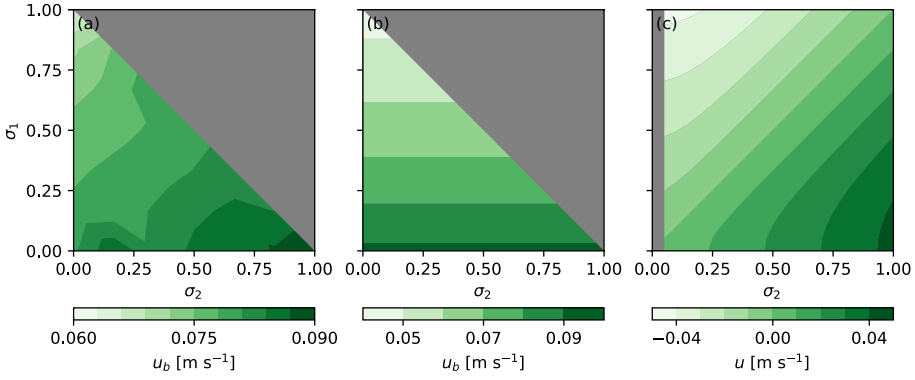


**Fig. 9** **a** Bottom front speed $u_b$ obtained from the numerical model for $\sigma_{glob} = -0.5$, as a function of $\sigma_2$ and $\sigma_1$. **b** As **a**, but $u_b$ is computed with Eq. 13 (that is, according to Linden [21]). **c** Intrusion front speed computed with Eq. 14 (that is, according to Maurer et al. [25]) as a function of $\sigma_2$ and $\sigma_1$. Note that for $\sigma_2 = 0$ this equation is not defined

ations. However, this formalism is not applicable to situations with a stratified lock since the level of neutral buoyancy is not uniquely determined from the initial conditions, given that the intrusion is stratified. Maurer et al. [25] generalize this formulation to a stratified lock, but restrict their work to cases with $\sigma_{glob} = 0$. They find for the front speed (their Eqs. (2.4) and (2.12))

$$u = 0.125 N_2 H \frac{1 - \frac{N_1^2}{N_2^2}}{\left(1 + \frac{N_1^2}{N_2^2}\right)^{\frac{1}{2}}}. \tag{14}$$

Figure 9c presents the front speeds from this equation. The dependence on stratification is qualitatively in line with our results for $\sigma_{glob} \neq 0$ (panel a), indicating that the found dependence of adjustment time on stratification extends to the case with $\sigma_{glob} = 0$.

Ungarish [40] used 1D shallow water equations for stratified currents and ambients. He found that front speed decreases with stronger stratification in the ambient and current. This apparent contradiction with our study is due to a difference in scaling of the initial conditions; if we scale in the same manner as Ungarish [40] the same dependency is found, underscoring the consistency with our theory. This also highlights the importance of accounting for the way dimensionless variables are obtained before drawing conclusions.

To summarize, the front speeds computed with the reduced model are in line with other studies, but additionally describe full-depth lock releases with stratification in the lock and ambient.

## 5 Discussion

We showed the effects of the horizontal density difference between the lock and the ambient, the stratification in the ambient and the stratification in the lock on the adjustment time of the lock exchange. Interactions of internal waves with the front motion have been described before [11, 27, 30]. We showed additionally that internal waves are important for the formation of a rarefaction wave and therefore to the equilibration process during the lock exchange, if the front speed is subcritical. The performance of the reduced model is considered good, given the simplifications performed to construct the model. The main assumptions are that the Froude number only depends on the horizontal density difference, and that the effects of stratification act on the initial hydrostatic pressure difference and on the internal wave speed. This first assumption is purely empirical, but is in line with Ungarish [40] and Goldman et al. [15]. The validity of the second assumption implies that other effects of stratification, like changing the vertical level at which an intrusion occurs or suppression of turbulence, are less important than the effect on the hydrostatic pressure. For values of $\sigma_{glob}$ closer to zero than considered in our study, the pressure differences are smaller and the vertical level of the intrusion may become more important, but the comparison with Maurer et al. [25] shows our theory extends to the lock exchange with $\sigma_{glob} \to 0$. To refine the reduced model, the description of the motion during and after the reflection could be improved, but this is considered beyond the scope of this study.

The use of the symmetry between the bottom and surface front in the reduced model avoids the need to make assumptions about energy conservation like in Shin et al. [37] or restrict the model to fronts which are small with respect to the water depth as in Ungarish [40]. Note that the heights of the fronts can be determined using volume conservation, that is,

$$u_b h = u_t(H - h), \tag{15}$$

in which $h$ is the height of the bottom front, and $u_b$ and $u_t$ are the front speeds of the bottom and surface current, respectively. Using front speeds determined from the numerical model output, Eq. 15 yields front heights in the range of $0.25\mathrm{H} - 0.75\mathrm{H}$, which compares well with the range of values simulated with the numerical model. However, care must be taken with the interpretation of these numbers, as Eq. 15 assumes that the currents travel at the bottom and surface boundaries, and therefore exclude intrusions, which do occur in the parameter space we consider. Moreover, an unambiguous determination of the front height in stratified conditions is not a trivial operation (see e.g. Borden and Meiburg [6]), and therefore no extensive analysis is performed for this quantity.

Our findings point out that neglecting stratification in either the ambient or the lock results in a poor approximation of adjustment times and associated quantities like front speeds, when the stratification is relatively strong with respect to the horizontal density gradient. After the adjustment time, changes to density of the lock are small. The extent to which the lock water has been replaced with ambient water depends on the initial conditions. In the supercritical case, most of the lock fluid (75% for the simulation of Fig. 5) is replaced by fluid from the ambient, except for a layer at the lock bottom, as revealed by the passive tracer (Fig. 10a). However, for the subcritical case, a substantial fraction of the lock fluid (48% for the simulation of Fig. 7) remains in the lock (Fig. 10b). It follows that exchanges with supercritical flow are more efficient in interchanging water between the lock and ambient than subcritical exchanges.

To give an example of a possible application of the developed theory, one can think of a situation where a contaminated water body exchanges with the environment, and the goal is to minimize the exchange. The ideal situation is a large adjustment time, and a weak exchange of fluid between the lock and ambient. If possible, it would therefore be advantageous to create a lock stratification which is just above the threshold for critical flow, where large adjustment times occur and the exchange is of the rarefaction wave type. Application

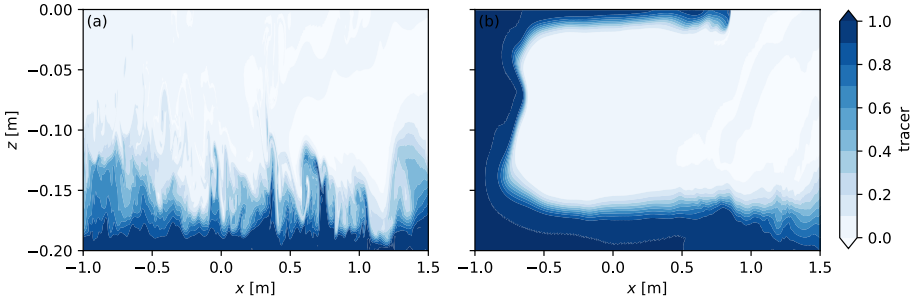


**Fig. 10** **a** Tracer field at $t = 60.0$ s for the simulation shown in Fig. 5. The tracer has initially a value of 1 for all $x < 0$ and a value of 0 elsewhere. **b** As **a**, but for the simulation shown in Fig. 7

to geophysical systems comes with additional complexity due to e.g. irregular bathymetry or other interacting currents. Also situations with a relatively simple geometry, like shipping locks, are more complicated than the laboratory settings considered in this study, due to the e.g. the presence of ships and leveling operations.

To gain more insight in the lock exchange with a stratified lock and ambient, future work could focus on determining the vertical density distribution in the surface and bottom fronts as a function of $\sigma_{glob}$, $\sigma_a$ and $\sigma_l$. A variety of conditions occur for this quantity, as e.g. in Fig. 5 the density of the bottom front resembles that of the lock, but compressed to a smaller vertical extent. But, in Fig. 7, the bottom front consists only of the fluid of the lower part of the lock. Understanding this density structure could be the first step to understand the front speeds from momentum and/or energy budgets. Another direction could be experimental work on the lock exchange with stratified lock and ambient (and a horizontal density difference). No published scientific work on this topic exists to the best knowledge of the authors. This will also be useful to extend the model validation beyond comparison of the front speeds.

## 6 Conclusions

The adjustment time, which is the timescale on which the density of a lock reaches steady conditions after a lock exchange, decreases for a larger density difference between lock and ambient. Presence of stratification, either in the lock or in the ambient, decreases the adjustment time. The internal wave speed is the velocity scale of the adjustment if the lock is strongly stratified (with respect to the horizontal salinity gradient). Otherwise, the speed of the front traveling into the lock is the relevant velocity scale. A reduced model reproduces the adjustment times computed with a detailed numerical model. The reduced model uses linear theory for internal wave speed [2] and generalizes solutions for front speeds in unstratified conditions found by Benjamin [3] to stratified locks and ambients, by assuming that the Froude number does not depend on stratification and that the main effect of stratification on front speed is by affecting the hydrostatic pressure. The density distributions after the lock release are important for improving the reduced model and could be the focus of future work.

## Appendix A Effect of the width of the initial transition layer

Mixing created by the removal of the vertical barrier in lock exchange experiments generates a mixed layer, with an expected width of a few centimeters. In our numerical model, this is accounted for by the parameter $L_{int}$, as defined in Sect. 2. Its value turned out to affect the strength of the Kelvin-Helmholtz billows that developed during the lock exchange. To illustrate this, Fig. 11 shows a simulation with identical conditions to those in Fig. 2a-e, except for the value of $L_{int}$, which is here 5 cm instead of 2 cm. It is visible that this simulation is associated with weaker Kelvin-Helmholtz billows, especially in the first half of the motion (panels b and c). To understand this, we compute the Richardson number *Ri* for the interface layer, which is a measure of flow stability. Flow is expected to develop strong turbulence for $Ri < 0.25$. In our two-dimensional setting, *Ri* is defined as

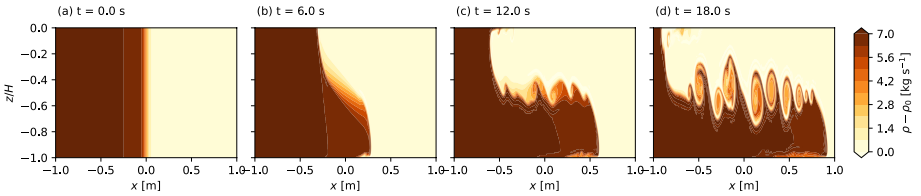


**Fig. 11** As Fig. 2b–e, but for $L_{int} = 5$ cm

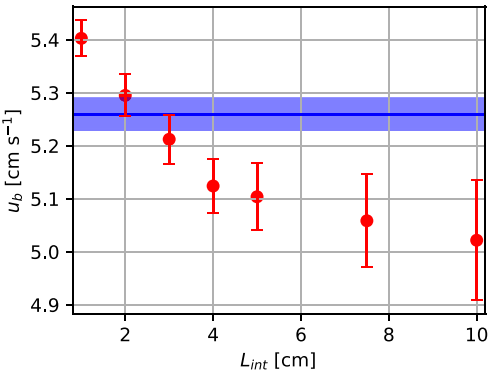


**Fig. 12** Bottom front speed $u_b$ as a function of interface width $L_{int}$. The blue line is the experimentally obtained value and the red dots are numerical simulations. The error bars and shaded area indicate one standard deviation

$$Ri = -\frac{g}{\rho_0}\frac{\frac{\partial \rho}{\partial z}}{(\frac{\partial v}{\partial z})^2}. \tag{A1}$$

where $v$ is the horizontal velocity component. If we assume that in the first stage of the lock exchange, the transition between the fluids tilts and becomes the separation between the surface and bottom currents, we can compute $Ri$. For the conditions in the Shin et al. [37] experiments, we have over the transition $\frac{\partial \rho}{\partial z} = \frac{\rho_l - \rho_a}{L_{int}}$ and $\frac{\partial v}{\partial z} = \frac{2u}{L_{int}}$. This yields $Ri = 0.13$ for $L_{int} = 2$ cm and $Ri = 0.33$ for $L_{int} = 5$ cm.

Based on these considerations, one would indeed expect strong turbulence production for $L_{int} = 2$ cm and weak turbulence for $L_{int} = 5$ cm, confirming the hypothesis that $L_{int}$ is important to the turbulence that develops in the simulations. Tests with different values of $L_{int}$ have however indicated that no sharp transition is present for $Ri = 0.25$.

One could argue based on these considerations that $L_{int} = 5$ cm is more appropriate to use for the simulations than $L_{int} = 2$ cm, as the turbulent motion in this simulation is closer to the experiments reported in Shin et al. [37]. However, a sensitivity analysis indicates that the front speed is lower for higher values of $L_{int}$, as shown in Fig. 12, and therefore has a worse agreement with the experiments in terms of front speed. Moreover, a mixed layer of 5 cm is intuitively too large to be generated by removal of the vertical barrier. Since the front speed turns out to be more important to the adjustment time than the amount of vertical mixing, we choose $L_{int} = 2$ cm, as this value gives the best agreement with the experiments in terms of front speed, keeping in mind that the flow in the model has more coherent turbulence structures than that observed in the experiments.

**Supplementary Information** The online version contains supplementary material available at https://doi.org/10.1007/s10652-026-10073-5.

**Acknowledgements** This work is part of the Perspectief Program SaltiSolutions, which is financed by NWO Domain Applied and Engineering Sciences (2022/TTW/01344701 P18-32 project2) in collaboration with private and public partners. We are grateful to Inge van Tongeren and Julie D. Pietrzak for their contributions to the first stage of this study.

**Author contributions** B.B. performed the simulations, analyzed the model output, produced the figures, devised the conceptual model and wrote the article draft. R.J.L. supervised the project, gave technical support for the numerical model, and reviewed the manuscript.

**Data availability** Model output generated for this study is available from the corresponding author upon reasonable request.

## Declarations

**Conflict of interest** The authors declare no Conflict of interest.



## References

1. Agrawal T, Peddada SH, Chalamalla VK (2022) Dynamics of a buoyant gravity current propagating in a linearly stratified medium. Phys Fluids 34(7):076605. https://doi.org/10.1063/5.0091683
2. Baines PG (2022) Topographic Effects in Stratified Flows, 2nd edn. Cambridge University Press, Cambridge, p 352. https://doi.org/10.1017/9781108481526
3. Benjamin TB (1968) Gravity currents and related phenomena. J Fluid Mech 31(2):209–248. https://doi.org/10.1017/S0022112068000133
4. Bonnecaze RT, Huppert HE, Lister JR (1993) Particle-driven gravity currents. J Fluid Mech 250:339–369. https://doi.org/10.1017/S002211209300148X
5. Bolster D, Hang A, Linden P (2008) The front speed of intrusions into a continuously stratified medium. J Fluid Mech 594:369–377. https://doi.org/10.1017/S0022112007008993
6. Borden Z, Meiburg E (2013) Circulation based models for boussinesq gravity currents. Phys Fluids 25(10):101301. https://doi.org/10.1063/1.4825035
7. Biemond B, Vuik V, Lambregts P, de Swart HE, Dijkstra HA (2024) Salt intrusion and effective longitudinal dispersion in man-made canals, a simplified model approach. Estuarine, Coastal Shelf Sci 298:108654. https://doi.org/10.1016/j.ecss.2024.108654
8. Caulfield CP (2021) Layering, instabilities, and mixing in turbulent stratified flows. Annual Rev Fluid Mech 53(2021):113–145. https://doi.org/10.1146/annurev-fluid-042320-100458
9. Cantero MI, Lee JR, Balachandar S, Garcia MH (2007) On the front velocity of gravity currents. J Fluid Mech 586:1–39. https://doi.org/10.1017/S0022112007005769
10. Dai A (2017) Experiments on two-layer density-stratified inertial gravity currents. Phys Rev Fluids 2:073802. https://doi.org/10.1103/PhysRevFluids.2.073802
11. Dai A, Huang Y-L, Hsieh Y-M (2021) Gravity currents propagating at the base of a linearly stratified ambient. Phys Fluids 33(6):066601. https://doi.org/10.1063/5.0051567
12. Garcia AMP, Geyer WR, Randall N (2022) Exchange flows in tributary creeks enhance dispersion by tidal trapping. Estuaries Coasts 45(2):363–381. https://doi.org/10.1007/s12237-021-00969-4
13. Garvine RW, Monk JD (1974) Frontal structure of a river plume. J Geophysical Res (1896–1977) 79(15):2251–2259. https://doi.org/10.1029/JC079i015p02251

14. Gladstone C, Ritchie LJ, Sparks RSJ, Woods AW (2004) An experimental investigation of density-stratified inertial gravity currents. Sedimentology 51(4):767–789. https://doi.org/10.1111/j.1365-3091.2004.00650.x
15. Goldman R, Ungarish M, Yavneh I (2014) Gravity currents with double stratification: a numerical and analytical investigation. Environ Fluid Mech 14:471–499. https://doi.org/10.1007/s10652-013-9288-1
16. He Z, Zhu R, Zhao L, Chen J, Lin Y-T, Yuan Y (2021) Hydrodynamics of weakly and strongly stratified two-layer lock-release gravity currents. J Hydraulic Res 59(6):989–1003. https://doi.org/10.1080/00221686.2020.1866690
17. James ID (2002) Modelling pollution dispersion, the ecosystem and water quality in coastal waters: a review. Environ Modell Softw 17(4):363–385. https://doi.org/10.1016/S1364-8152(01)00080-9
18. Johnson CG, Hogg AJ (2013) Entraining gravity currents. J Fluid Mech 731:477–508. https://doi.org/10.1017/jfm.2013.329
19. Khodkar M, El Allam K, Meiburg E (2018) Intrusions propagating into linearly stratified ambients. J Fluid Mech 844:956–969. https://doi.org/10.1017/jfm.2018.218
20. Kokkinos A, Prinos P (2023) On the dynamics of gravity current motion in a stratified ambient. J Hydraulic Res 61(5):703–719. https://doi.org/10.1080/00221686.2023.2239749
21. Linden P (2012) Gravity currents theory and laboratory experiments. In: Buoyancy-Driven Flows. Cambridge University Press, Cambridge, pp 13–50. Chap. 1. https://doi.org/10.1017/CBO9780511920196.002
22. Labeur RJ, Wells GN (2007) A Galerkin interface stabilisation method for the advection diffusion and incompressible Navier Stokes equations. Comput Methods Appl Mech Eng 196(49):4985–5000. https://doi.org/10.1016/j.cma.2007.06.025
23. Labeur RJ, Wells GN (2009) Interface stabilised finite element method for moving domains and free surface flows. Comput Methods Appl Mech Eng 198(5):615–630. https://doi.org/10.1016/j.cma.2008.09.014
24. Labeur RJ, Wells GN (2012) Energy stable and momentum conserving hybrid finite element method for the incompressible Navier Stokes equations. SIAM J Sci Comput 34(2):889–913. https://doi.org/10.1137/100818583
25. Maurer BD, Bolster DT, Linden P (2010) Intrusive gravity currents between two stably stratified fluids. J Fluid Mech 647:53–69. https://doi.org/10.1017/S0022112009993752
26. McSweeney SL, Kennedy DM, Rutherfurd ID (2018) The daily-scale entrance dynamics of intermittently open/closed estuaries. Earth Surf Proc Land 43(4):791–807. https://doi.org/10.1002/esp.4280
27. Maxworthy T, Leilich J, Simpson JE, Meiburg EH (2002) The propagation of a gravity current into a linearly stratified fluid. J Fluid Mech 453:371–394. https://doi.org/10.1017/S0022112001007054
28. MacVean LJ, Stacey MT (2011) Estuarine dispersion from tidal trapping: A new analytical framework. Estuaries Coasts 34(1):45–59. https://doi.org/10.1007/s12237-010-9298-x
29. Marino BM, Thomas LP, Linden PF (2005) The front condition for gravity currents. J Fluid Mech 536:49–78. https://doi.org/10.1017/S0022112005004933
30. Munroe JR, Voegeli C, Sutherland BR, Birman V, Meiburg EH (2009) Intrusive gravity currents from finite-length locks in a uniformly stratified fluid. J Fluid Mech 635:245–273. https://doi.org/10.1017/S0022112009007563
31. Nasr-Azadani MM, Meiburg E (2016) Gravity currents propagating into ambients with arbitrary shear and density stratification: vorticity-based modelling. Q J R Meteorol Soc 142(696):1359–1370. https://doi.org/10.1002/qj.2739
32. Nicoud F, Ducros F (1999) Subgrid-scale stress modelling based on the square of the velocity gradient tensor. Flow Turbul Combust 62(3):183–200. https://doi.org/10.1023/A:1009995426001
33. Ooi SK, Constantinescu G, Weber LJ (2007) 2D Large-eddy simulation of lock-exchange gravity current flows at high Grashof numbers. J Hydraul Eng 133(9):1037–1047. https://doi.org/10.1061/(ASCE)0733-9429(2007)133:9(1037)
34. Orton PM, Jay DA (2005) Observations at the tidal plume front of a high-volume river outflow. Geophys Res Lett. https://doi.org/10.1029/2005GL022372
35. Rijnsburger S, Flores RP, Pietrzak JD, Horner-Devine AR, Souza AJ (2018) The influence of tide and wind on the propagation of fronts in a shallow river plume. J Geophys Res Oceans 123(8):5426–5442. https://doi.org/10.1029/2017JC013422
36. Rottman JW, Simpson JE (1983) Gravity currents produced by instantaneous releases of a heavy fluid in a rectangular channel. J Fluid Mech 135:95–110. https://doi.org/10.1017/S0022112083002979
37. Shin JO, Dalziel SB, Linden PF (2004) Gravity currents produced by lock exchange. J Fluid Mech 521:1–34. https://doi.org/10.1017/S002211200400165X
38. Simpson JE (1999) Gravity Currents: In the Environment and the Laboratory, 2nd edn. Cambridge University Press, Cambridge

39. Ungarish M (2009) An Introduction to Gravity Currents and Intrusions, 1st edn. Chapman and Hall/CRC, Boca Raton, p 488. https://doi.org/10.1201/9781584889045
40. Ungarish M (2012) Gravity currents and intrusions of stratified fluids into a stratified ambient. Environ Fluid Mech 12(2):115–132. https://doi.org/10.1007/s10652-011-9216-1
41. Wu C-S, Dai A (2020) Experiments on two-layer stratified gravity currents in the slumping phase. J Hydraulic Res 58(5):831–844. https://doi.org/10.1080/00221686.2019.1671517
42. Zhu R, He Z, Meiburg E (2023) Mixing, entrainment and energetics of gravity currents released from two-layer stratified locks. J Fluid Mech. https://doi.org/10.1017/jfm.2023.146